J Mater Sci: Mater Electron (2012) 23:1235–1242
DOI 10.1007/s10854-011-0580-x

Some physical properties and Vickers hardness measurements of Fe diffusion-doped $Bi_{1.8}Pb_{0.35}Sr_{1.9}Ca_{2.1}Cu_3O_y$ superconductors

O. Ozturk

Received: 16 August 2011 / Accepted: 14 November 2011 / Published online: 20 November 2011

Abstract In this study we have investigated the influence of iron diffusion and diffusion-annealing time on the mechanical and the superconducting properties of bulk $Bi_{1.8}Pb_{0.35}Sr_{1.9}Ca_{2.1}Cu_3O_y$ superconductors by performing X-ray diffraction (XRD), scanning electron microscopy (SEM), Vickers hardness, dc resistivity (ρ-T) and critical current density (J_c) measurements. The samples are prepared by the conventional solid-state reaction method. Doping of Bi-2223 was carried out by means of iron diffusion during sintering from an evaporated iron film on pellets. Then, the Fe layered superconducting samples were annealed at 830 °C for 10, 30 and 60 h. The mechanical properties of the compounds have been investigated by measuring the Vickers hardness (H_v). The mechanical properties of the samples were found to be load dependent. The load independent Vickers hardness (H_0), Young's modulus (E), yield strength (Y), and fracture toughness (K_{IC}) values of the samples are calculated. These all measurements showed that the values of the Vickers hardness, critical current density, and critical transition temperature and lattice parameter *c* increased with increasing Fe doping and diffusion-annealing time.

1 Introduction

Since the discovery of the high temperature oxide superconductors, extensive study has been done in order to improve their superconducting and structural properties. Among the cuprate superconductors, the *Bi*-based cuprates (BSCCO) attract great interest not only because of their physical properties but also due to practical applications such as fabrication of long lengths wire and tapes. BSCCO superconductors are discovered by Maeda et al. [1]. The BiSrCaCuO system mainly contains three phases under the general formula $Bi_2Sr_2Ca_{n-1}Cu_nO_{2n+4+x}$ where $n = 1,2$ and 3 refer to the number of CuO_2 layers and their superconducting transition temperatures (T_c) are about 20, 85 and 110 K, respectively [2–5]. Among them Bi-2223 system is the most attractive because it has the highest transition temperature.

As part of a study of doping, the effect of additions of oxides such as SiO_2, Al_2O_3, ZnO_2, MgO_3 and 3d translation metal oxides on $YBaCu_3O_{7-x}$ (YBCO) [6, 7] and $(Bi\,Pb)_2Sr_2Ca_2Cu_3O_{10-y}$ (BSCCO) [8] have been investigated. Among the metals Au and Ag have been found to be non-poisoning to YBCO [9], while Ag has been found to be the only metal element that is non-poisoning to the BSCCO system [10]. In our previous works, the role of diffusion annealing time and temperature on the superconducting, structural and mechanical properties of Au diffusion-doped Bi-2223 superconductors were investigated [11–15]. These works indicated that gold doping enhance the superconducting and the mechanical properties of the samples. And we have recently investigated the effect of substitution of Sm for Ca in Bi-2223 superconductors on superconducting, micro-structure and mechanical properties [16, 17]. We found that superconducting and mechanical properties degrade with increasing Sm content.

Engineering applications of high temperature superconducting ceramics are generally restricted because of their brittleness nature, therefore improvement of the mechanical properties of BSCCO is a major research

O. Ozturk (✉)
Department of Physics, Faculty of Arts and Science, Kastamonu University, 37100 Kastamonu, Turkey
e-mail: oozturk@kastamonu.edu.tr

objective and very important for their practical applications. Hardness is a mechanical parameter and it is strongly related to the structure and composition of solids. The Vickers microhardness test is one of the convenient methods to estimate the mechanical properties [18]. In our recent study, we have investigated the effect of iron diffusion-doping on the superconducting and mechanical properties of Bi-2223 superconductors [19]. The results of that study indicated that iron diffusion-doping improved the superconducting and mechanical properties. We have used three empirical models to analyze the load dependent microhardness and indentation size effect (ISE). In this study, we focus further analyze the ISE behavior using two different methods on the same samples used in the previous work [19]. We also calculate Young's modulus (E), yield strength (Y), and fracture toughness (K_{IC}) values of the samples.

2 Results and discussion

The samples of $Bi_{1.8}Pb_{0.35}Sr_{1.9}Ca_{2.1}Cu_3O_y$ pellets will be hereafter denoted as F0 (undoped sample annealed at 830 °C for 10 h), F1 (iron diffused sample annealed at 830 °C for 10 h), F2 (iron diffused sample annealed at 830 °C for 30 h), and F3 (iron diffused sample annealed at 830 °C for 60 h). Sample preparation process was mentioned in our previous study [19].

2.1 XRD characterization

XRD data results of samples taken from our previous work [19] are summarized in Table 1. The diffusion of Fe resulted in an increase of the lattice parameter *c* of the sample. The increase in lattice parameter *c* revealed that cations of the system (Bi^{+3}, Sr^{+2}, Ca^{+2}) might partly be substituted by Fe ions. Formation of Bi-2223 phase is enhanced by Fe doping, and the volume ratio of 2223 phase further increases with annealing-diffusion time. The intensities of the peaks for the Fe doped samples are higher than those of the un-doped sample which reveals the enhancement of grain growth and better orientation of grains with Fe diffusion.

2.2 SEM observations

The surface morphologies of the Fe-diffused and pure samples were studied by using a JEOL 6390-LV scanning electron microscope (SEM) to determine the grain sizes and possible precipitation at the grain boundaries. Figure 1 represents surface micrographs for the F0, and F3 samples. The F0 sample consists of flake-like grains and the grains are oriented randomly and poorly connected as shown in Fig. 1. The flake-like grains are believed to be due to the Bi-2212 phase [20, 21]. The flake-like grains are less dominant in sample F3 in comparison with F0 sample, while the concentration of the needle-like grains grew gradually. The needle-like grains are believed to be due to

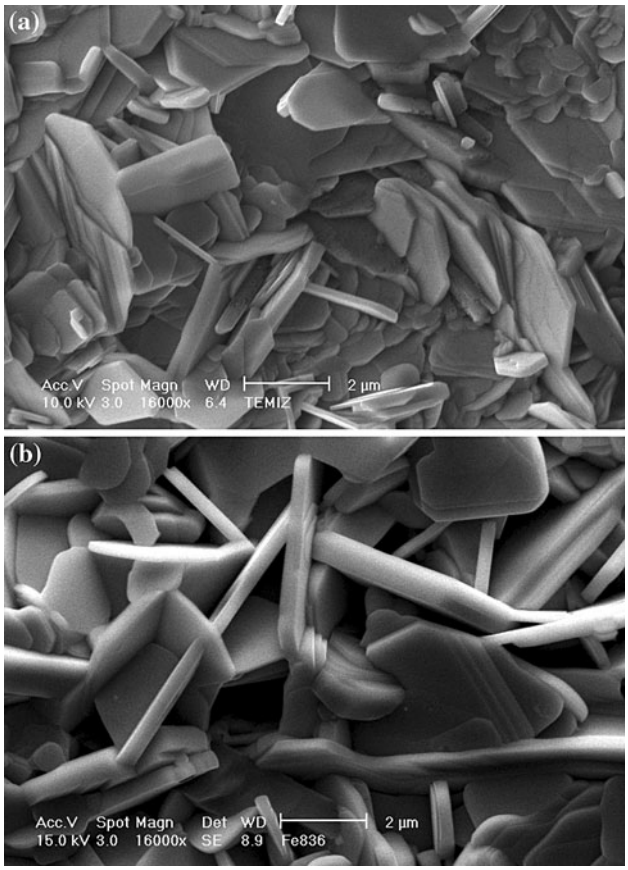

Fig. 1 SEM measurements of the **a** F0, **b** F3 samples

Table 1 Critical temperature (T_c), critical current density (J_c), lattice parameters *a* and *c*, and volume fraction values for the samples

Samples	T_c^{offset} (K)	$\%V_{2223}$	$\%V_{2212}$	*a* (°A)	*c* (°A)	J_c (A/cm^2)
F0	100.0 ± 0.2	66.00	34.00	5.431	36.96	32.5
F1	106.0 ± 0.2	74.30	25.70	5.391	37.00	50.0
F2	106.5 ± 0.2	81.70	18.30	5.380	37.10	56.2
F3	107.0 ± 0.2	88.20	11.80	5.373	37.16	65.0

the Bi-2223 phase [20–22]. Moreover, XRD examination results to support these observations. The surface morphology of the sample is relatively improved by Fe-doping. F0 has non-uniform surface appearance with smaller grains. Iron film on the sample forms a metallic connection; this resistive short-circuit connects the grains and lowers the room temperature resistivity. This effect continues even when iron film is diffused into the sample, indicating the iron's effect on grain boundary properties. SEM pictures show better connectivity in iron coated samples after heat treatment at 830 °C for 60 h. All SEM pictures of samples were shown in our previous study [19].

2.3 Electrical measurements

The measurements of dc resistivity and critical current density (J_c) were performed with the four-probe method on all samples. Both voltage and current contacts were made with silver paint, the contact resistance being in the order of 0.1 Ω or lower. The temperature dependence of resistivity of the samples are measured in the range 90–130 K with 5 mA dc current through the samples in the cryostat. A Keithley 220 programmable current source and a Keithley 2182A nano-voltmeter were used for the resistivity and I–V measurements. We determined J_c from the I–V curves at liquid nitrogen temperature (77 K), following the 1 μV/cm criteria.

The temperature dependence of normalized resistivity for all samples (F0, F1, F2 and F3) is shown in Fig. 2. The temperature dependence of the resistivities of the samples shows the metallic behavior above the onset temperature. Zero-resistivity transition temperatures of the samples are determined as 100, 106, 106.5 and 107 K, respectively. The estimated T_c values of the samples increased with increasing Fe content. The transition width of the samples decreased with increasing annealing time. The F0 and F1 samples were annealed isothermally at 830 °C for 10 h. As can be seen from the figure that the transition curves from the normal to the superconducting state have double step nature which is more pronounced in F0. We believed that the double step resistive transition could be related to the impurity phases which may play role weak links at the grain boundaries [23]. It is observed that the zero resistivity transition temperature of the F1 (106 K) is higher than that for the F0 sample (100 K). The increase in T_c may be related to the optimization of the hole concentration and possible changes in the lattice vibration of Bi(Pb)-Sr-Ca-Cu-O. It can be seen from the figure that the broadening of the resistivity transition width of the F1 sample is smaller than that for the F0 sample. It is also possible that resistive nature of the grain boundaries is modified by accumulation of iron atoms at the grain boundaries. Although wetting of the grain boundaries by a very thin layer of iron is unlikely, preferential accumulation of iron ions at the grain boundaries may reduce the resistive behavior. The critical current densities as a function of iron diffusion and diffusion annealing time were measured in liquid nitrogen at zero magnetic fields. Resistive contacts caused heating and the test was completed in possible shortest time, in order to avoid this effect. An I–V curve for the samples is shown Fig. 3. The calculated J_c values of all samples are summarized in Table 1. It is observed that the J_c of the samples increases from 32.5 to 65 A/cm^2 with increasing the iron doping and diffusion annealing time. The increase of J_c in the samples may be caused by the increase of grain sizes and by improved coupling between superconducting grains [24].

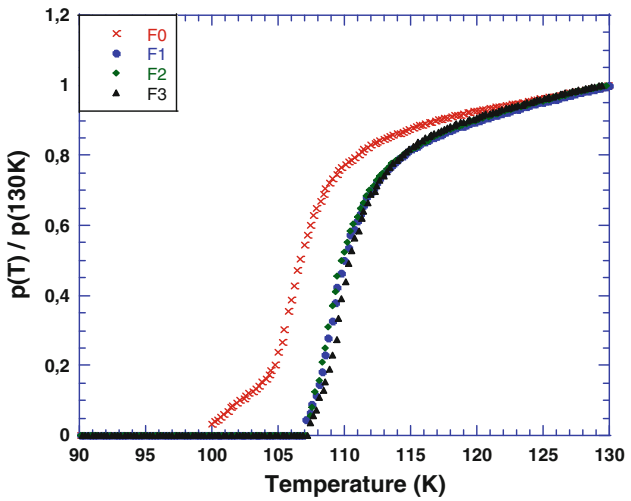

Fig. 2 Normalized resistivity as a function of temperature measurements of F0, F1, F2 and F3 samples

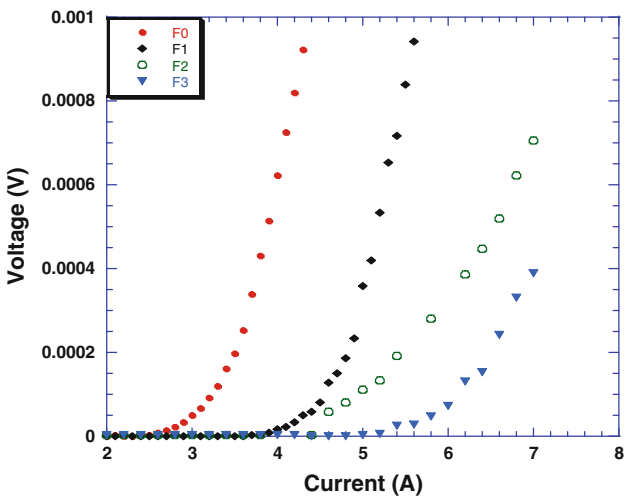

Fig. 3 I–V measurements of F0, F1, F2 and F3 samples

2.4 Mechanical characterization

Hardness measurements of BSCCO samples were performed on polished surfaces with a digital microhardness tester (Instron Series 2100) at room temperature. A Vickers pyramidal indenter with different loads (0.245, 0.490, 0.980, 1.960, and 2.940 N) and a single loading time of 10 s were applied and the diagonals of indentation were measured with an accuracy of ±0.1 μm. Indentations were made at different parts of the samples' surface in such a way that the distance between any two indentations was no less than two times the diagonal of the indentation mark to avoid surface effects due to neighboring indentation. An average of 10 readings at different locations of sample surfaces was taken to obtain reasonable mean values for each load.

The Vickers microhardness (apparent) values of different applied loads were calculated by using the equation [25]

$$H_v = 1854.4 \left(F/d^2\right) (GPa) \quad (3)$$

where F is the applied load in Newton (N) and d is the diagonal length of the indentation mark in μm. The calculated load dependent microhardness values for different applied loads are summarized in Table 2. Figure 4 displays the variation of microhardness as a function of the applied load for the F0, F1, F2, and F3 samples. The variation of microhardness with load has similar shape irrespective of the Fe doping although numerical values are different. We have observed that the microhardness values increased with increasing diffusion-annealing time. The reason of this is ascribed to Fe doping (diffusion) filling the intergrain space, resulting in better grain growth and causing larger grains, as a result, leading to a remarkable increase in the mechanical resistance of the samples. It was observed that Vickers hardness increased with increasing amount of doping in Bi-2223 superconductors [17, 20, 26, 27]. The rapid variation of microhardness was observed with increasing applied load from 0.245 to 0.980 N. The reason for this behaviour is due to the contribution of weak grain boundaries [22]. Vickers microhardness values are load dependent for all samples; the calculated microhardness value decreases non-linearly as the applied load decreased until 0.980 N, then it tends to attain saturation. As reported by Khalil [20, 40], this behavior can be explained as following; (a) at larger indention loads, the Vickers hardness registered smaller values, this observation may be due to the presence of weak grain boundaries of the superconducting ceramics; (b) at smaller indention loads, the Vickers hardness recorded higher values, this is ascribed to the fact measured hardness values were more indicative of the monocrystalline state without interference from grain boundaries. This non-linear behavior has also been observed in the literature for Bi-Pb-Sr-Ca-Cu-O samples [17, 20, 28] and is known as indentation size effect (ISE) [29–32].

Table 2 The calculated load dependent H_v, E, Y and K_{IC} values for the samples

Samples	Load (N)	d (μm)	H_v (GPa)	E (GPa)	Y (GPa)	K_{ic} (Pa/m$^{1/2}$)
F0	0.245	31.50	0.458	37.53	0.153	490.9
	0.490	53.50	0.317	26.02	0.106	408.8
	0.980	83.30	0.262	21.47	0.087	371.3
	1.960	122.1	0.244	19.98	0.081	357.0
	2.940	151.0	0.239	19.60	0.079	354.8
F1	0.245	29.30	0.529	43.36	0.176	538.8
	0.490	51.00	0.349	28.61	0.116	437.6
	0.980	75.00	0.323	26.47	0.108	421.0
	1.960	107.1	0.316	25.90	0.105	416.4
	2.940	134.2	0.302	24.75	0.101	407.1
F2	0.245	28.10	0.575	47.13	0.192	599.9
	0.490	49.40	0.378	30.98	0.126	486.3
	0.980	74.70	0.325	26.64	0.108	451.0
	1.960	106.2	0.322	26.39	0.107	448.9
	2.940	131.5	0.315	25.82	0.105	444.0
F3	0.245	26.00	0.672	55.08	0.224	679.5
	0.490	45.50	0.438	35.90	0.146	548.6
	0.980	69.05	0.381	31.23	0.127	511.6
	1.960	100.1	0.362	29.67	0.121	498.7
	2.940	123.1	0.359	29.42	0.120	496.6

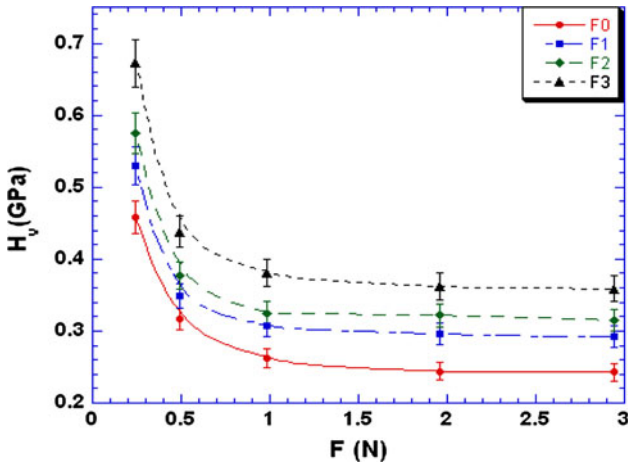

Fig. 4 Vickers microhardness versus applied indentation load

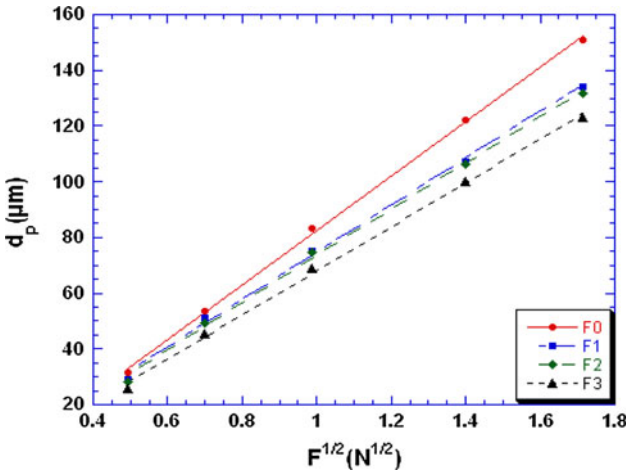

Fig. 5 Plots of diagonal length versus square root of applied loads for the samples

To account for this effect, several relationships between the applied load and the resulting indentation size have been suggested [33–36]. This effect can be explained by two different methods [25]. The first method assumes that the indentation contains an elastic portion. The elastic part of the deformation is relaxed upon loading. This can be accounted for by adding an elastic component, d_e, to the measured plastic indentation semidiagonal, d_p. Thus, a true hardness, H_0, is defined from Refs. [25, 37]

$$H_0 = 1854.4\left(\frac{F}{(d_p + d_e)^2}\right)(GPa) \tag{4}$$

Therefore, Eq. 4 indicates that measured indentation diagonals should be linear with the square root of the applied load and the slope of such a curve is proportional to $(H_0)^{1/2}$ and the vertical intercept of this graph is proportional to the elastic part of the indentation semi diagonal, d_e. The load dependence of indentation diagonals for F0, F1, F2 and F3 samples was reanalyzed as d_p versus $F^{1/2}$ plots, as in Fig. 5. The extracted values of H_o, d_e and LRC are listed in Table 3. As can be seen from the table, it was observed that the values of H_o of the samples increased slightly with increasing the diffusion-annealing time. As can be seen from Table 3, true microhardness value of F0 sample (0.194 GPa) is lower than the hardness results (see Table 2) in the plateau region (saturated region) ($H_v = 0.239$ and 0.243 GPa). This behavior is observed in other samples (F1, F2 and F3) in this work. The value of d_e is 15.21 μm for F0 sample and in the range of 9.98–10.81 μm for Fe doped samples (F1, F2 and F3).

The second method considers energy dissipative processes during the indentation rather than elastic processes. In this model, a true microhardness can be defined by subtracting a dissipative part, F_0, from the applied load [25]

Table 3 Best fit results of experimental data according to Eq. 4

Samples	H_0 (GPa)	d_e (μm)	LRC	H_v (GPa)
F0	0.194	15.21	0.9995	0.239–0.243
F1	0.261	9.979	0.9990	0.302–0.315
F2	0.267	10.47	0.9987	0.315–0.321
F3	0.298	10.81	0.9991	0.359–0.361

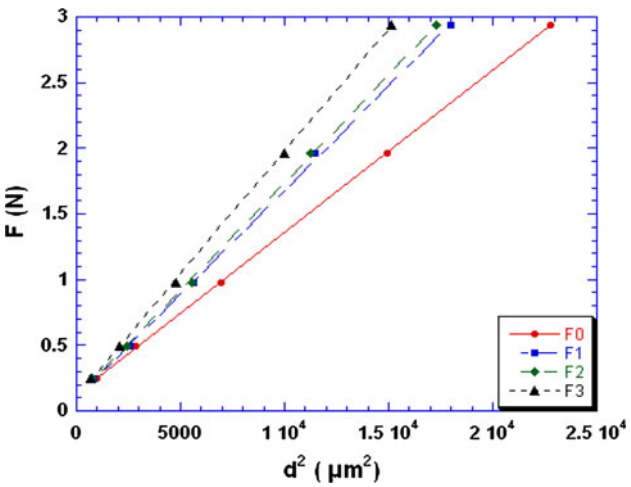

Fig. 6 Graph of the applied load against the square of the diagonal length for the samples

$$H_0 = 1854.4\left(\frac{F - F_0}{d^2}\right)(GPa) \tag{5}$$

Figure 6 exhibits applied load as a function of the square of the diagonal length for the samples. Each set of data shows an excellent linear relationship (LRC $\succ$ 0.99996). The slope of each line corresponds to the load independent hardness constant, H_0 and the intercept of each line represents the sample resistance pressure, F_0. The extracted

Table 4 Best fit results of experimental data according to Eq. 5

Samples	H_0 (GPa)	F_0 (N)	LRC	H_v (GPa)
F0	0.123	0.128	0.9999	0.239–0.243
F1	0.158	0.097	0.9997	0.302–0.315
F2	0.164	0.093	0.9998	0.315–0.321
F3	0.186	0.104	0.9999	0.359–0.361

Table 5 Best fit results of experimental data according to Eq. 6

Samples	H_0 (GPa)	$\gamma \times 10^{-3}$ (N/μm)	LRC	H_v (GPa)
F0	0.100	3.191	0.9952	0.239–0.243
F1	0.135	3.348	0.9926	0.302–0.315
F2	0.137	3.818	0.9998	0.315–0.321
F3	0.152	4.192	0.9916	0.359–0.361

values of F_0, H_0 and LRC were listed in Table 4. As can be seen from this table, the values of H_0 for the iron doped samples increased with increasing the diffusion-annealing time and the LRC of each sample is very high, implying that Eq. 5 provides a satisfactory description of the indentation data for the samples.

On the other hand, it is observed that the diagonal length is strongly dependent on the applied load. This observation is governed by

$$\frac{F}{d} = H_0 d + \gamma \tag{6}$$

proposed in [17, 33, 38, 39]. Figure 7 exhibits the values of F/d against the diagonal length of indentation, d, for the samples. The slope of each line corresponds to the true hardness, H_0 and the intercept of each line represents the surface energy, γ. The extracted values of H_0, γ and LRC were listed in Table 5. The values of H_0 and γ of the samples increased with increasing the diffusion-annealing time. This observation is ascribed to the dissipation of the energy of cracks at the interfaces [25] and a similar behavior in ceramics was also reported in indentation works [17, 39, 40].

In most materials, the elastic modulus (Young's modulus), E, is related to the Vickers microhardness (apparent) by the relation [41]

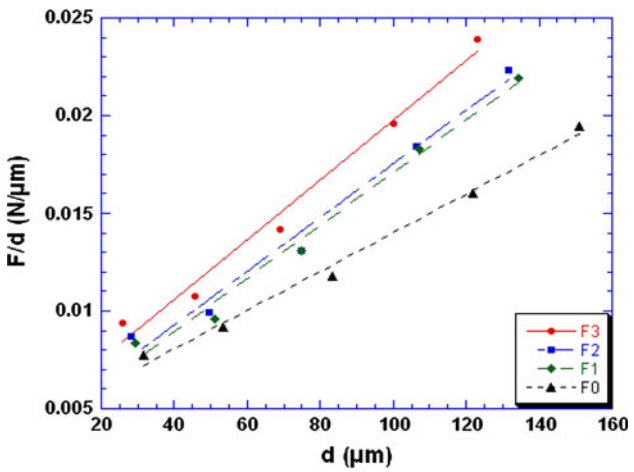

Fig. 7 Plots of F/d versus d for the samples

$$E = 81.9635\, H_v \tag{7}$$

and yield strength Y is related to the hardness by the relation [42, 43]

$$Y \approx H_v/3 \tag{8}$$

The value of load dependent E and Y were calculated for each load by using Eqs. 7 and 8, and summarized in Table 2. As seen in this table, the load dependent E and Y increase significantly with increasing diffusion-annealing time and decreasing loads. This behavior is due to crack initiation and improvement of microhardness. Similar changes in the yield strength and elastic modulus were reported in the literature [41]. This indicates that the diffusion-annealing hardens the superconductor materials further with longer durations.

It is useful to mention the fracture toughness, K_{IC}, as it is one of the main mechanical properties of superconducting samples. The fracture toughness is an important parameter for the selection of materials for applications. Due to the nature of intrinsic brittleness, microindentation may result in microfracture around the impressed region on the surface of the samples. Since microfracture occurs mainly during the loading a portion of the energy, which is used to create the indentation deformation, will be dissipated by the crack formation. Owing to the definition of the K_{IC} as the critical stress intensity factor, it is directly related to γ of the crack faces [44]

$$K_{IC} = \sqrt{2E\gamma} \tag{9}$$

where E is the load dependent Young's modulus. The values of load dependent K_{IC} were calculated by using Eq. 9 and summarized in Table 2. From this table, it is observed that K_{IC} increases significantly with increasing diffusion-annealing time and decreasing loads. Similar change in the fracture toughness was reported in the literature [40]. Owing to this relation, an increase in K_{IC} corresponds to an increase in the average surface energy as proposed from the hardness calculations.

In addition, we focused on load independent values of Young's modulus, yield strength and fracture toughness of the samples. Instead of using apparent microhardness (H_v) values to calculate load dependent Y, E and K_{IC} in Eqs. 7–9 for each load, one can calculate E, Y and K_{IC} using true

Table 6 The calculated load independent H_v, E, Y and K_{IC} values for the samples

Samples	H_0 (GPa)	E (GPa)	Y (GPa)	K_{ic} (Pa/m$^{1/2}$)
F0	0.100	8.196	0.033	228.7
F1	0.135	11.06	0.045	272.1
F2	0.137	11.22	0.046	292.7
F3	0.152	12.45	0.050	323.0

microhardness (load independent, H_0) calculated by Eq. 6 for each sample. The obtained load independent Y, E and K_{IC} for the samples are tabulated in Table 6. From the table, it was observed that the load independent values of E, Y, K_{IC} increase significantly with increasing the diffusion annealing duration. Comparing Tables 2 and 6, one can conclude that the load dependent values are higher than that of load independent values. This is in agreement with the literatures [11, 25]. The above results revealed that by increasing the diffusion-annealing duration, it is possible to control the mechanical properties of the samples.

3 Conclusion

A microindentation method can be used to measure mechanical properties of polycrystalline superconductors such as hardness, Young's modulus, yield strength, and fracture toughness. Our measurements showed that the increase of diffusion-annealing time improved mechanical and superconducting properties of the samples. When Fe-doped samples of $Bi_{1.8}Pb_{0.35}Sr_{1.9}Ca_{2.1}Cu_3O_y$ phase, prepared by solid-state reaction methods, are compared with those for the undoped sample, following statements are concluded for doped samples:

- The lattice parameter c and high-T_c phase (Bi-2223) increase by iron doping with increasing diffusion-annealing time.
- The critical transition temperature (T_c) increases.
- Room temperature resistivity decrease with increasing diffusion-annealing time.
- The critical current density (J_c) enhances.
- The microstructure of the surface morphology is improved with increasing Fe diffusion-doping.
- The improvement of superconducting properties is due to the modification of grain boundaries together with better crystallinity and larger grains by iron doping with increasing diffusion-annealing time.
- The improvement of mechanical properties can be observed by the increase of microhardness with increasing diffusion-annealing time.
- The estimated apparent microhardness, Young's modulus, yield strength and fracture toughness values of the samples are load dependent. Their variation with load is non-linear.
- The ISE behaviour is examined by Eqs. 4 and 5. Equation 4 is found to be more suitable for describing the experimental data.
- The load independent H_0, E, Y and K_{IC} can be calculated directly using Eq. 6.
- The load dependent values of H_v, E, Y and K_{IC} are greater than that of load independent values.

References

1. H. Maeda, Y. Tanaka, M. Fukutomi, T. Asano, Jpn. J. Appl. Phys. **27**(2), L209 (1988)
2. L. Gao, J.Z. Huang, L.R. Meng, H.P. Hor, J. Bechtold, Y.Y. Sun, W.C. Chu, Z.Z. Chen, M.A. Herman, Nature **332**, 623 (1988)
3. W.C. Chu, J. Bechtold, L. Gao, H.P. Hor, J.Z. Huang, L.R. Meng, Y.Y. Sun, Y.Q. Wang, Y.Y. Zue, Phys. Rev. Lett. **60**, 941 (1988)
4. L.J. Tallon, G.R. Buckley, W.P. Gilbert, R.M. Presland, M.W.I. Brown, E.M. Bowder, A.L. Christan, R. Gafull, Nature **333**, 153 (1988)
5. H. Abbasi, J. Taghipour, H. Sedghi, J. Alloys Compd. **482**, 552–555 (2009)
6. S.X. Dou, H.K. Lin, A.J. Bourdillon, J.P. Zhou, N.X. Tan, X.Y. Sun, C.C. Sorrell, J. Am. Ceram. Soc. **71**, 329 (1988)
7. S.X. Dou, N. Savides, X.Y. Sun, A.J. Bourdillon, C.C. Sorrell, J.P. Zhou, K.E. Easterling, J. Phys. C: Solid State Phys. **20**, 1003 (1987)
8. S.X. Dou, H.K. Liu, S.J. Guo, K.E. Easterling, J. Mickeel, Supercond. Sci. Technol. **2**, 274 (1990)
9. G. Xion, F.H. Streitz, M.Z. Cieplak, A. Bakhshei, A. Gourin, C.L. Chien, Phys. Rev. B **38**, 776 (1988)
10. S. Jin, R.C. Sherwood, T.H. Tiefel, G.W. Kammlott, Appl. Phys. Lett. **52**, 1628 (1998)
11. M. Yilmazlar, O. Ozturk, O. Gorur, I. Belenli, C. Terzioglu, Supercond. Sci. Technol. **20**, 365–371 (2007)
12. O. Ozturk, T. Küçükömeröğlu, C. Terzioglu, J. Phys, Condens. Matter **19**, 346205 (2007)
13. C. Terzioglu, O. Ozturk, I. Belenli, J. Alloys Compd. **471**, 142–146 (2009)
14. O. Ozturk, M. Akdogan, C. Terzioglu, A. Gencer, J. Phys. Conf. Ser. **153**, 012024 (2009)
15. O. Ozturk, C. Terzioglu, I. Belenli, J. Supercond. Nov. Magn. **24**, 381–390 (2011)
16. C. Terzioglu, M. Yilmazlar, O. Ozturk, E. Yanmaz, Physica C **423**, 119 (2005)
17. M. Yilmazlar, H.A. Cetinkara, M. Nursoy, O. Ozturk, C. Terzioglu, Physica C **442**, 101 (2006)
18. M. Yilmazlar, O. Ozturk, H. Aydın, M. Akdogan, C. Terzioglu, Chinese J. Phys. **45**(2-I), 128–134 (2007)
19. O. Ozturk, H.A. Cetinkara, E. Asikuzun, M. Akdogan, M. Yilmazlar, C. Terzioglu, J. Mater. Sci.: Mater. Electron **22**, 1501–1508 (2011)
20. S.M. Khalil, J. Phys. Chem. Solids **62**, 457 (2001)
21. Y.C. Chen, K.K. Chong, T.H. Meen, Jpn. J. Appl. Phys. **30**, L33 (1991)
22. K.H. Yoon, Y.B. Lee, J. Mater. Sci. **26**, 5101 (1991)
23. P. Kameli, H. Salamati, M. Eslami, Solid State Commun **137**, 30–35 (2006)
24. O. Ozturk, D. Yegen, M. Yilmazlar, A. Varilci, C. Terzioglu, Physica C **451**, 113–117 (2007)

25. A. Leenders, M. Ullrich, H.C. Freyhardt, Physica C **279**, 173 (1997)
26. E. Bruneel, J. Degrieck, I. Van Driessche, S. Hoste, Physica C **1063**, 372–376 (2002)
27. H.C. Ling, M.F. Yan, J. Appl. Phys. **64**, 1307 (1988)
28. A. Murakami, K. Katagiri, K. Noto, K. Kasaba, Y. Sohoji, M. Muralidhar, N. Sakai, M. Murakami, Physica C **794**, 378–381 (2002)
29. J. Gong, J. Wu, Z. Guan, Mater. Lett. **38**, 197 (1999)
30. K. Sangwal, B. Surowska, Mater. Res. Innov. **7**, 91 (2003)
31. R. Tickoo, R.P. Tandon, K.K. Bamzai, P.N. Kotru, Mater. Chem. Phys. **42**, 446 (2003)
32. A.A. Elmustafa, D.S. Stone, J. Mech. Phys. Solid **51**, 357 (2003)
33. F. Fröhlinch, P. Grau, W. Grellmann, Phys. Status Solid **42**, 79 (1997)
34. H. Li, R.C. Bradt, J. Mater. Sci. **22**, 917 (1993)
35. C. Hays, E.G. Kendall, Metallography **6**(4), 275 (1973)
36. J. Gong, J. Wu, Z. Guan, J. Eur. Ceram. Soc. **19**, 2625 (1999)
37. Z. Li, A. Ghosh, A.S. Kobayashi, J. Am. Soc. **72**, 904 (1989)
38. K. Hirao, M. Tomozawa, J. Am. Ceram. Soc. **70**, 497 (1997)
39. E.O. Bernhardt, Z. Metall. **33**, 135 (1941)
40. S.M. Khalil, Smart Mater. Struct. **14**, 804 (2005)
41. C. Veerender, V.R. Dumke, M. Nagabhooshanam, Phys. Status Solid A **144**, 199 (1994)
42. F.A. McClintock, A.S. Argon, *Mechanical behaviour of materials* (Addison-Wesley, Reading, 1996), p. 455
43. D. Tabor, *The hardness of metals* (Clarendon, Oxford, 1951)
44. B.Y. Farber, N.S. Sidorov, V.I. Kulakov, A.Y. Lunin, A.N. Izotov, G.A. Emel'chenko, V.S. Bobrov, L.S. Fomenko, V.D. Natsik, S.V. Lubenets, Superconductivity **4**, 2296 (1991)